Supplementary Information

Laterally Swept Light-sheet Microscopy Enhanced by Pixel Reassignment for Photon Efficient Volumetric Imaging

LIANG QIAO,[1,†] HONGJIN LI,[1,2,†] SUYI ZHONG,[3,†] XINZHU XU,[3] FEI SU,[1,4] PENG XI[1,3], DAYONG JIN[1,4,*], KARL ZHANGHAO,[1,*]

[1] UTS-SUSTech Joint Research Centre for Biomedical Materials and Devices, Department of Biomedical Engineering, College of Engineering, Southern University of Science and Technology, Shenzhen, Guangdong 518055, China
[2] Department of Biomedical Engineering, City University of Hong Kong, Hong Kong, China
[3] Department of Biomedical Engineering, College of Future Technology, Peking University, Beijing 100871, China
[4] Institute for Biomedical Materials and Devices (IBMD), Faculty of Science, University of Technology Sydney, NSW 2007, Australia
†These authors contributed equally to this work.

*Corresponding authors: dayong.jin@uts.edu.au, karl.hao.zhang@gmail.com

---

Table of contents

Supplementary Figure 1: Comparison of the light sheets between ASLM and LSLM with simulation studies at N.A.=0.5

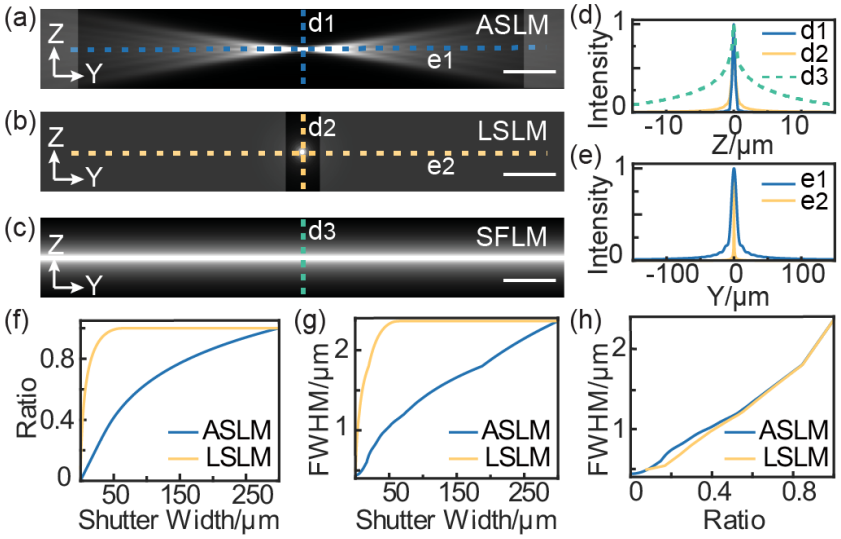

Fig. S1. Simulation of light-sheet generation in axially swept light-sheet (ASLM), laterally swept light-sheet (LSLM), and swept focus light-sheet microscopy (SFLM) over a volume of 300 μm × 300 μm × 300 μm with N.A.=0.5, *n*=1.33, λ=473 nm. (a, b) Cross-sectional view of the light sheet with a cropped Y-FoV of 100 μm in the Y-Z plane after first scanning for ASLM in (a) and for LSLM in (b). Scale bar: 10 μm. **(c)** Cross-sectional view of SFLM in the Y-Z plane generated by lateral and axial scanning without confocal detection. **(d)** The intensity profiles along Z-axis for d1 in (a), d2 in (b), and d3 in (c). The FWHM is 440 nm for ASLM, 490 nm for LSLM, and 2.37 μm for SFLM. **(e)** The intensity profiles along Y-axis for e1 in (a) and e2 in (b). **(f)** The energy ratio changes with rolling shutter widths for both ASLM and LSLM. **(g)** The axial FWHM increases with larger rolling shutter width for both ASLM and LSLM. **(h)** The relationship between axial FWHM and energy ratio.

Supplementary Figure 2: The performance of iLSLM under different conditions with simulation studies

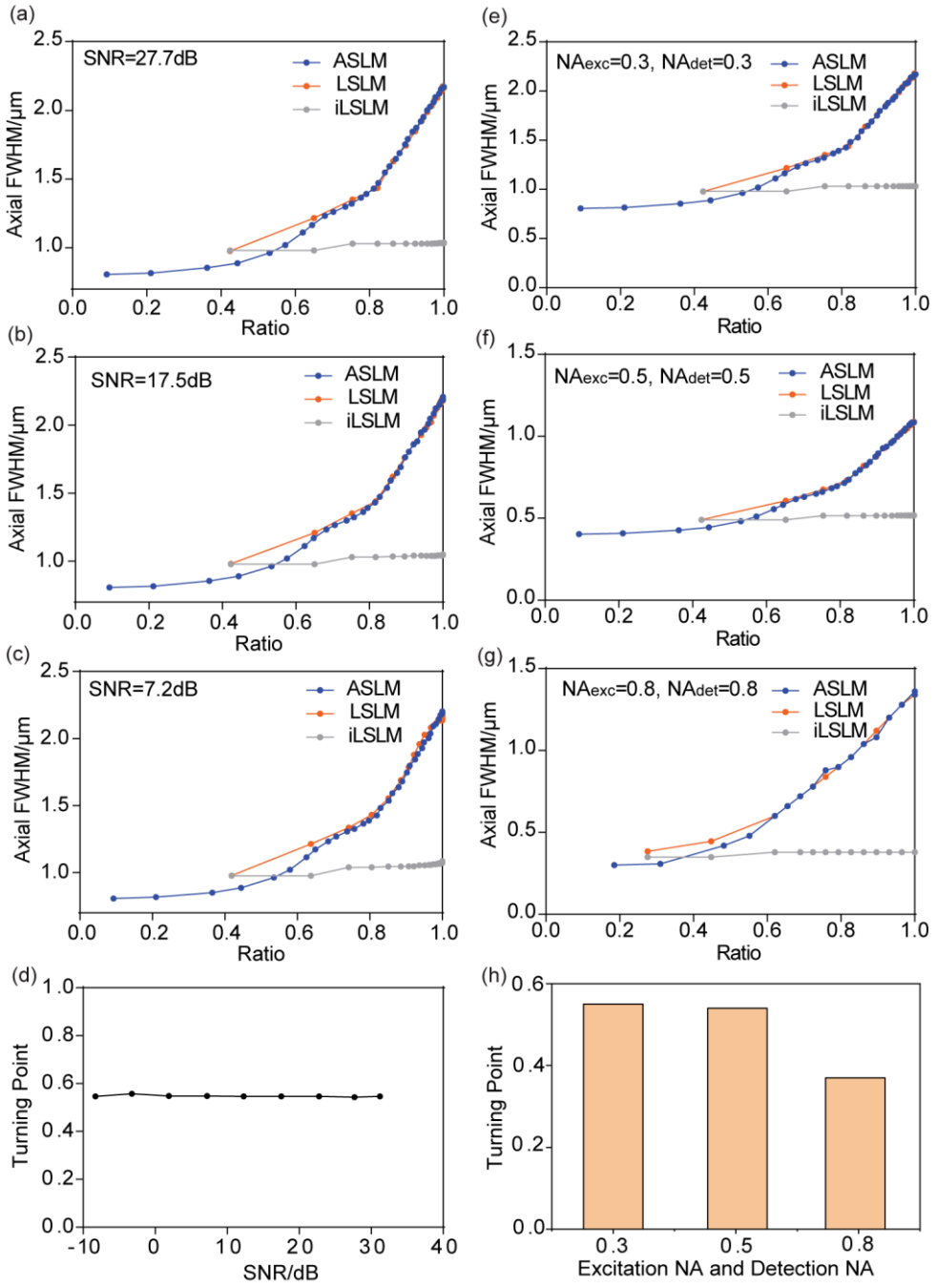

Fig. S2 Comparison of the performance among ASLM, LSLM, and iLSLM under different conditions. In our experiments, the iLSLM is superior to ASLM in axial FWHM at 55% photon efficiency in the simulation results and at 53% photon efficiency in the experimental results. The "turning point" is consistent in the simulation and the experiments although their signal-to-noise (SNR) ratio is quite different. **(a-d)** We simulate how the SNR will influence the "turning point". The different levels of Gaussian noise (SNR = 7.2dB, 17.5dB, 27.7dB) were added to the raw images and then analyzed following the schedules of ASLM, LSLM, and iLSLM. (a-c) shows the axial FWHM of ASLM, LSLM, iLSLM ($N.A._{exc}$ = 0.3 and $N.A._{det}$ = 0.3) plotted with different photon efficiencies under different SNR levels. (d) plots the turning point with the SNR. The results show that the SNR does not influence the "turning point". We believe the "turning point"

remains the same because the noise affects the ASLM and LSLM results similarly. Here the SNR is calculated with an open-source Fiji plug-in (SNR_.jar from the Biomedical Image Group of EPFL), based on the following equation:

$$SNR = 10 \cdot lg\left[\frac{\sum_0^{n_x-1}\sum_0^{n_y-1}[r(x,y)]^2}{\sum_0^{n_x-1}\sum_0^{n_y-1}[r(x,y)-t(x,y)]^2}\right]$$

Where n_x, n_y is image coordinate position, $r(x,y)$ is the image needed to calculate SNR, $t(x,y)$ is the reference image. **(e-f)** We conduct simulated studies to study how the N.A. influences the "turning point". The "turning point" is 55% when $N.A._{exc} = 0.3$ and $N.A._{det} = 0.3$, 54% when $N.A._{exc} = 0.5$ and $N.A._{det} = 0.5$, and 37% when $N.A._{exc} = 0.8$ and $N.A._{det} = 0.8$. The "turning point" will become smaller as the objective N.A. increases, which indicates that the iLSLM is more advantageous when higher N.A. objective is used.

Supplementary Figure 3: Comparison of the excitation powers in the light-sheet microscopy with different scanning modes

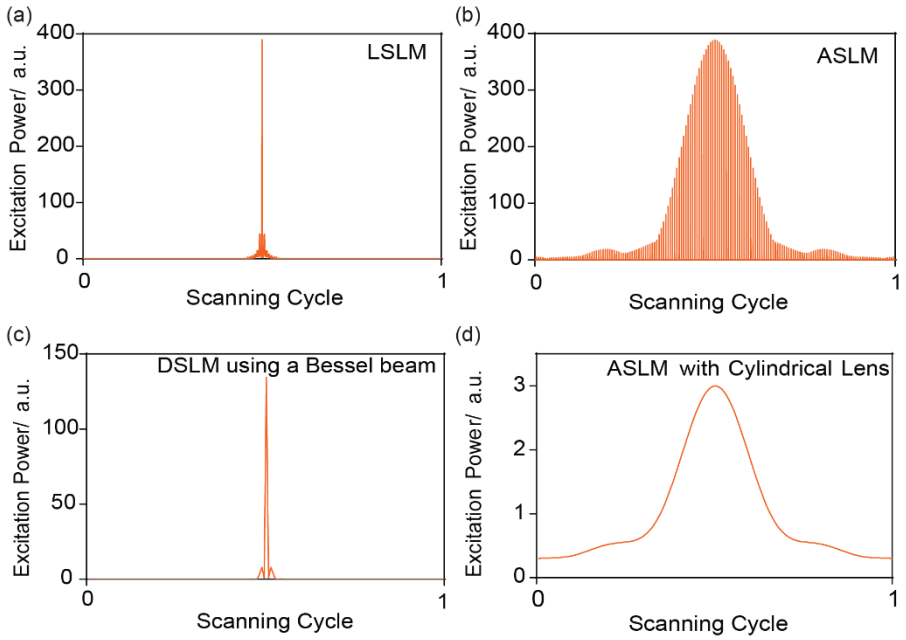

Fig. S3. The duty cycle or excitation power during one scanning cycle is studied for different types of light sheet microscopy. Here, the "scanning cycle" from 0 to 1 means from the start to the end of the scanning, while different numbers of scanning are used during one scanning cycle for various types of light sheet microscopy. The integration of the excitation power during one scanning cycle are also normalized to 1 arbitrary unit (a.u.) for a fair comparison. Although the scanning of the light sheets enhances the imaging performance, it increases the peak excitation power because the specimen is excited for only a small portion of the whole scanning cycle. In other words, the scanning of the light sheets reduces the duty cycle of excitation. The peak excitation power or duty cycle is an important influencing factor when discussing photobleaching or phototoxicity. If the peak power falls into the nonlinear regime, severe photobleaching or photobleaching will happen. The LSLM/iLSLM technique developed here is to image the specimen susceptible to photobleaching or phototoxicity, so low excitation power is used to keep the peak excitation power within the linear regime.

(a) The Gaussian light sheet (N.A.=0.3) is scanned in the LSLM mode, which is firstly axially scanned and then laterally swept. **(b)** The Gaussian light sheet (N.A.=0.3) is scanned in the ASLM mode, which is firstly laterally scanned and then axially swept. The duty cycle of LSLM and ASLM is the same because only the scanning order is different in the two modes. **(c)** The digital scanned light sheet microscope (DSLM) using a Bessel beam ($N.A._{in} = 0.18$, $N.A._{out} = 0.3$) slightly reduces the peak excitation power and increases the duty cycle. **(d)** The ASLM uses a cylindrical lens to form a light sheet instead of lateral scanning, followed by the axially swept, which significantly reduces the peak intensity power. Nevertheless, the light sheet generated with a cylindrical lens is usually less uniform compared with the scanned light sheet.

Supplementary Note 1: Sample preparation

Fluorescent beads: First, we mix 1.1 mL of deionized water and 2.2 μL of 200 nm fluorescent beads (F8888, Thermofisher) by sonication for 3 min, and heat up the mix to 90°C. We dissolve 10 mg of agarose powder (A0701-25g, Aldrich) in 1 mL of the mixed solution at 90°C for 5 min, use a pipette gun to mix them well, and keep them at 90°C for another 5 min to obtain the sample solution. Then we use a capillary glass tube with a piston rod to draw a certain amount of the sample solution, and push them out for imaging after solidification. Note that the prepared samples need to be kept at 4 ℃ away from light.

U2OS Cells: U2OS cells (ATCC, USA) are cultured in Dulbecco's Modified Eagle's medium (DMEM, GIBCO, USA) containing 10% heat-inactivated fetal bovine serum (FBS, GIBCO, USA) and 100 U/ml penicillin and 100 μg/ml streptomycin solution (PS, GIBCO, USA) at 37°C in an incubator with 95% humidity and 5% CO2. For the cell imaging, 1h before imaging, U2OS cells are labeled with 1 μg/ml Nile Red (N1142, Invitrogen, USA), mixed with melted 1% agarose, and then drawn inside a glass capillary (1 mm diameter) and pushed out for imaging after solidification.